Available online at www.sciencedirect.com
SCIENCE DIRECT
Polymer 46 (2005) 1653–1660
polymer
www.elsevier.com/locate/polymer

Tensile properties of polyethylene-layered silicate nanocomposites

Maged A. Osman, Jörg E.P. Rupp, Ulrich W. Suter*

Department of Materials, Institute of Polymers, ETH, CH-8093 Zurich, Switzerland

Received 21 September 2004; accepted 22 November 2004
Available online 21 December 2004

Abstract

The sodium ions of clays with different cation exchange capacities (CEC) have been exchanged with alkyl ammonium ions, in which 1–4 octadecyl chains are attached to the nitrogen atom. Due to the different cation cross-sectional area to available area per cation ratio, the resulting organo-montmorillonites (OMs) have different organic surface coverage and alkyl chain packing density. Nanocomposites of these OMs and HDPE were prepared and the influence of the organic monolayer structure on the exfoliation of montmorillonite and the tensile properties of the composites was studied. A high cation cross-sectional area to available area ratio led to complete surface coverage and large *d*-spacing, favoring the dispersion of the filler. In spite of the identical chemical structure of the polymer and the organic monolayer, complete exfoliation was not attained. Partial exfoliation was achieved without a compatiblizer, which often adversely affect the mechanical properties of the composites. Enhanced exfoliation increased the elastic modulus and yield stress but decreased the yield strain and stress at break of the nanocomposites. Increased filler loading enhanced the elastic modulus but decreased all other tensile properties. The tensile properties were correlated to the volume fraction of the inorganic part of the OMs and not to the total volume of the OM. Fitting the elastic modulus data to the Halpin-Tsai equation showed that the fitting parameter in this equation is not only related to the aspect ratio of the inclusions.

Keywords: Nanocomposite; Polyethylene-montmorillonite; Tensile properties

1. Introduction

Polyethylene with almost one third of the world plastic production is one of the most popular polymers. It is often compounded with natural minerals to enhance its stiffness, toughness, dimensional-stability and electric-insulation properties [1,2]. A prerequisite for reinforcement is optimal filler dispersion (agglomerate disintegration) and spatial distribution in the polymer matrix. The properties of the composites are determined by those of the components, shape, and volume fraction of the filler as well as by the morphology of the system and the nature of the interphase that sometimes develop at the interface of the two components. Although there is no direct correlation between the filler particle size and the composite properties, it plays an important role due to the increase in surface area of the inclusions and decrease of the interparticle distance with decreasing particle diameter. The aspect ratio of the inclusions also strongly influences the tensile properties [3,4]. Generally, the elastic modulus increases with augmenting filler volume fraction, while all other tensile properties such as the yield stress and strain, the ultimate stress, and strain almost invariably decrease with increasing filler volume fraction [5–9].

Models developed to predict the moduli (M) of composites are mainly based on either hydrodynamic considerations, e.g. Guth-Smallwood (1), or on continuum solid mechanics, e.g. the Kerner equation and its modifications such as Hashin-Shtrikman or Halpin-Tsai (2) [10–16].

$$\frac{M}{M_1} = 1 + 2.5\phi_2 + 14.1\phi_2^2 \tag{1}$$

where ϕ is the volume fraction and the subscripts 1 and 2 denote the continuous and the dispersed phase, respectively. It should be noted that this model assumes spherical shape for the randomly distributed inclusions.

* Corresponding author. Tel.: +41 44 632 2039; fax: +41 44 632 1592.
E-mail address: uwsuter@eth.ch (U.W. Suter).

0032-3861/$ - see front matter © 2004 Elsevier Ltd. All rights reserved.
doi:10.1016/j.polymer.2004.11.112

$$\frac{M}{M_1} = \frac{1 + AB\phi_2}{1 - B\phi_2} \tag{2}$$

where A is a parameter that reflects the reinforcement geometry (particle shape and orientation), packing geometry and loading conditions. A has different expressions for different composite moduli and is a unique function of Poisson's ratio of the matrix in each case. For oriented discontinuous ribbon or lamella-shaped reinforcement, Halpin [14–16] estimated A to be twice the aspect ratio. B is a parameter that takes the moduli of the filler and the matrix into account (3) and its value is one for very large filler/matrix ratio, which is the case in polymers filled with natural minerals.

$$B = \frac{(M_2/M_1) - 1}{(M_2/M_1) + A} \tag{3}$$

It is to be remarked that all models, which predict the mechanical properties of composites, assume perfect adhesion between the two heterogeneous phases. This is not necessarily true in the case of surface treated fillers.

For the composition dependence of the yield stress and stress at break, different empirical models have been proposed. The simplest model for describing the tensile strength (σ) of filled polymers is that presented by Nicolais and Nicodemo [17]:

$$\frac{\sigma}{\sigma_1} = 1 - b\phi^a \tag{4}$$

where b is a constant related to stress concentrations ($b=1.21$ for spherical particles having no adhesion) and a is a constant related to the geometry of the particles ($a=2/3$ when the sample fails by random fracture, which is the common case). However, the predicted σ is considered as a lower bound response and the upper bound is more difficult to predict because it depends on quantitative information regarding the adhesion between the polymer and the filler.

Polymer-layered silicate nanocomposites are nanoscale organic–inorganic hybrid materials, in which the inclusions have at least one dimension smaller than 100 nm. That is, the aluminosilicate platelets offer a combination of high aspect ratio and large surface area, which have consequences for the composite properties. Due to strong interactions between the nanoparticles and the polymer matrix (resulting from the huge surface area), and decreased interparticle distances, significant morphological changes occur. This leads to improvements in the permeation-barrier behavior, thermal stability and flame retardency as well as in the mechanical and dielectric properties at low loading [18–22]. Smectites, especially montmorillonite, which can be exfoliated to highly anisometric 1 nm thick layers, have been frequently used to prepare polymer nanocomposites. To render its hydrophilic surface compatible with the mostly hydrophobic polymers, favoring exfoliation and intercalation, its inorganic cations (Na^+) are usually exchanged with organic ions to give organo-montmorillonite (OM) [23,24].

Polyethylene-OM nanocomposites have been prepared by melt-compounding or in situ intercalative polymerization and some of their mechanical properties were reported [25–30]. In the case of melt-compounding, the filler dispersion is often poor and the use of a compatibilizer, usually maleic anhydride-grafted PE, is necessary to achieve exfoliation. The resulting composites are usually stiffer than the pristine polymer but no general trends for the other tensile properties can be gained from the scarce results described in the literature. PE-nanocomposites prepared by in situ intercalative polymerization are more homogeneous and partial exfoliation is achieved but their tensile properties were generally poor because of low degrees of polymerization. The general trends observed in the tensile properties of other polymer-nanocomposites with increasing loading are: enhanced stiffness, morphology dependent tensile strength, and reduced ultimate elongation [20,31,32].

Actually, the aspect ratio of the inclusions in polymer-OM nanocomposites depends mainly on their thickness (extent of exfoliation), which in turn depends on the interactions between the OM and the polymer. Generally, interplay of entropic and energetic factors governs the exfoliation and intercalation processes [33]. Theoretical studies showed that the miscibility between the two phases is a function of the Flory-Huggins interaction parameter ($\chi \lesssim 0$ is required) [34–36]. The alkyl chains are supposed to completely mask the silicate surface, increase the basal-plane spacing (d-spacing), and indefinitely mix with the polymer chains. Grafting chains, which are chemically identical to those of the polymer, to the silicate surface does not guarantee complete wetting because of the autophobicity, which may occur [37]. That is, exfoliation requires an optimal structure of the organic monolayer with respect to the alkyl chain length and molecular cross-section of the organic cation. Differences in enthalpic interactions and entropic packing effects have to be balanced by the entropy of mixing. It has been predicted that loose as well as too dense packing of the alkyl chains in the surfactant monolayer is unfavorable for forming hybrids [34]. For linear high molecular weight polymers like PE, an intercalated morphology without exfoliation at best ($\chi \lesssim 0$) was prophesied. The packing density and phase behavior of alkyl chains attached to aluminosilicate surfaces have been studied and shown to be a function of chain length and ratio of molecular cross-section to available area per cation [38,39].

The objective of the present investigation is to study the influence of the clay surface coverage and alkyl chains packing density on the exfoliation of the OMs in polyethylene and consequently on the tensile properties of the nanocomposites. For this purpose, the inorganic cations of clays with different CEC were exchanged by alkyl ammonium ions, in which different numbers (1–4) of octadecyl chains are attached to the nitrogen atom. A correlation between the tensile properties of these composites and the inorganic volume fraction as well as with the

aspect ratio of the inclusions is also targeted. Since, the inorganic part of the OM is that which contributes to the reinforcement, only its volume fraction is correlated to the tensile properties of the composites and not the total volume of the OM.

2. Experimental part

2.1. Starting materials and composites

Sodium montmorillonites with different cation exchange capacities (CEC): Nanofil 757, Optigel CK and Optigel CMO, were supplied by Süd-Chemie AG (Moosburg, Germany). Cloisite Na was purchased from Southern Clay Inc. (Gonzales, TX, USA). Octadecyltrimethylammonium chloride (C18), methyltrioctadecylammonium bromide (3C18) and tetraoctadecylammonium bromide (4C18) were procured from Fluka (Buchs, Switzerland), while dioctadecyldimethylammonium bromide (2C18) was purchased from Acros Organics (New Jersey, USA). The polyethylene used is linear high density PE (Hostalen GF 9055F) that was supplied by Basell (Mainz, Germany). It has a density of 0.954 g/cm^3 (23 °C) and a melt flow index of 0.5 g/10 min (2.16 kg at 190 °C). The montmorillonite surface treatment and nanocomposite synthesis have been described elsewhere [24,39,46]. In contrast to commercial OMs, the prepared fillers do not contain excessive ammonium salts. The required amounts of OM and HDPE to obtain the desired inorganic volume fraction were calculated as previously described [46].

2.2. Transmission electron microscopy (TEM)

The microstructure of the nanocomposites was studied by bright-field TEM using a Zeiss LEO-912 Ω microscope, acceleration voltage 120 KV. Pieces of the 60 μm films were etched with oxygen plasma for 3 min and embedded in an epoxy matrix (Epon 812 + Durcopan ACM 3:4; Fluka, Buchs, Switzerland). Sections (50–100 nm thick) were microtomed at −150 °C with a diamond knife (Reichert Jung Ultracut E). The sections were supported by 100 mesh grids sputter-coated with 3 nm thick carbon layer.

2.3. Wide angle X-ray diffraction (WAX)

Wide-angle X-ray diffraction patterns were collected on a Scintag XDS 2000 diffractometer (Scintag Inc., Cupertino, CA) using Cu K_α radiation ($\lambda = 0.15406$ nm) in reflection mode. The instrument was equipped with a graphite monochromator and an intrinsic germanium solid-state detector. The films and OMs were step-scanned (step width 0.02° 2Θ, scanning rate 0.06°/min) at room temperature from 1.5 to 10° 2Θ. The (001) basal-plane reflection of an internal standard muscovite ($2\Theta = 8.84°$) was used to calibrate the line position of the sample reflections. To determine the peak positions, the diffractograms were fitted with a split Pearson VII function (diffraction management system software 1.36b).

2.4. Tensile testing

Engineering stress–strain curves were obtained from uniaxial tension tests (ISO 527-2) on dumbbell-shaped tensile bars of type 5B stamped out of the compression molded plaques. The measurements were carried out at room temperature on a Zwick Z020 tensile tester with testXpert 9.01 software (Zwick, Ulm, Germany). The displacement was measured with a Video-Extensometer V4.19.02 (Messphysik, Fürstenfeld, Austria). The elastic modulus was determined at 0.1 mm/min crosshead speed (0.05–0.25% strain), while all other tensile characteristics were measured at 6 mm/min. An average of at least five measurements for each sample is reported.

3. Results and discussion

The inorganic cations of clays with different CEC were exchanged by alkyl ammonium ions, in which different numbers (1–4) of octadecyl chains are attached to the nitrogen atom. The OMs were free of excessive ammonium salts that are usually present in commercial OMs, which adversely affect the thermal stability and mechanical properties of the composites [40–42]. The alkyl ammonium ions were chosen on the basis of the identical chemical structure of the alkyl chains and the PE chains, in order to obtain similar surface energies. Table 1 summarizes the clay types used, their CEC, the organic cations exchanged in each case, and gives acronyms for the resulting OMs. The area per cation available on the montmorillonite surface decreases with increasing CEC, while the cross-sectional area of the cation increases with augmenting number of alkyl chains attached to the nitrogen atom. This leads to a high chain packing density and complete surface coverage in 4C18·M900 and 3C18·M1000, but low packing density and incomplete surface coverage in C18·M680. With increasing packing density, the chains adopt essentially all-*trans* conformation and an upright position, in which the average molecular axis is tilted to the surface normal. The tilt angle decreases with increasing number of chains in the cation, leading to larger *d*-spacing [39]. Table 2 gives the measured *d*-spacing of the OMs, showing that for the same cation the basal-plane spacing increases with rising CEC. For the same clay, the *d*-spacing increases with growing number of alkyl chains attached to the nitrogen atom. In other words, the basal-plane spacing is a function of the ratio of molecular cross-sectional area to the available area per cation. With increasing distance between the aluminosilicate layers, the attraction forces between them diminish. An appreciable *d*-spacing of 3.5–4 nm was measured for the highly charged clay surfaces treated with tri- and

Table 1
CEC of the clays, area per cation and acronyms for the OMs

Clay	CEC [μeq/g]	Area/cat. [nm^2]	C18	2C18	3C18	4C18
Nanofil 757	680	1.87	C18·M680	2C18·M680	3C18·M680	
Cloisite Na	880	1.44		2C18·M880	3C18·M880	
Optigel CK	900	1.41	C18·M900	2C18·M900	3C18·M900	4C18·M900
Optigel CMO	1000	1.27	C18·M1000	2C18·M1000	3C18·M1000	

Table 2
Basal-plane spacing of the organo-montmorillonites

Montmorillonite	*d*-spacing [nm]			
	C18	2C18	3C18	4C18
M680	1.82	2.45	3.25	
M880		2.51	3.48	
M900	1.85	2.66	3.58	3.94
M1000	2.14	3.28	3.84	

tetraoctadecyl ammonium ions, which is favorable for exfoliation. The *d*-spacing in the PE-OM nanocomposites was found to be the same as that of the corresponding OM powder, which indicates that the polymer was not intercalated in the gaps between the layers (interlayer) of the OM. As an example, the WAX patterns of 1-3C18·M680 are compared to those of their 2.8 vol% PE composites in Fig. 1, showing that no shift in the peak positions occurred. The (001) peak width in 2C18·M680-HDPE is larger than in the other two modifications probably due to differences in the tactoids thicknesses and in the coherence length of the crystalline domains (several tactoids). The coherence length is influenced by the compounding and processing conditions as well as by the sample preparation; therefore the tactoids thickness cannot be deduced from the peak width. The increased intensity of the composite reflections is mainly due to better orientation of the tactoids in the composite films than in the OM powder. Since the orientation of the tactoids could not be monitored, we refrained from using the peak area to quantify the degree of exfoliation. In spite of the similarity in chemical structure of the polymer and the organic monolayer covering the montmorillonite surface, no polymer intercalation was observed. However, transmission electron microscopy (TEM) showed that partial exfoliation occurred and single silicate layers as well as thin tactoids were seen, i.e. a mixed morphology (exfoliated layers + OM tactoids) is present (Fig. 2).

The tensile properties of the 2.8 vol% HDPE-OM nanocomposites are summarized in Table 3. All composites are stiffer than the neat polymer but the modulus enhancement differs according to clay type and surface treatment. The relative elastic modulus of the composites (composite/polymer) is plotted in Fig. 3 as a function of the *d*-spacing. As can be seen, the modulus steadily increases with augmenting *d*-spacing. Since, the stiffness is a function of the inclusions aspect ratio and the increase in *d*-spacing of the OM does not increase its aspect ratio, no direct correlation between the basal-plane spacing and the modulus can be expected [43]. A reasonable explanation for the observed dependence is that larger *d*-spacing leads to decreased attraction between the silicate layers, which can be overcome by the shear forces during compounding. This leads to more exfoliated silicate layers with high aspect ratio, which has been observed by TEM (Fig. 2). That is, increased *d*-spacing facilitates the exfoliation, resulting in modulus enhancement. Although OMs with high cation cross-sectional area to available area per cation ratio have *d*-spacing 3–4 nm (Table 2), they were not completely exfoliated. This is probably because the free energy of mixing the two heterogeneous phases is still high and the attraction forces between the layers decrease asymptotically with increasing *d*-spacing. The attraction between the layers also depends on their surface area, that is, the large platelets adhere stronger than small ones. The shear forces in the kneader used seem to be not high enough to overcome the residual attraction between all platelets. It should be recalled that no polymer intercalation was observed, although partial delamination took place. It may be that the dispersion is not thermodynamically stable as theoretically predicted and the

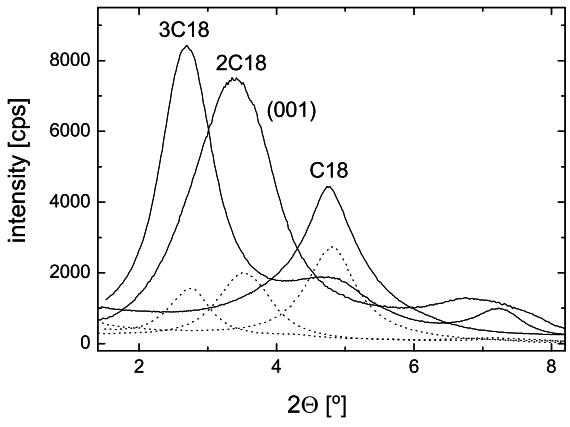

Fig. 1. WAX patterns of 1-3C18·M680 (dotted lines) and their 2.8 vol% HDPE composites (solid lines).

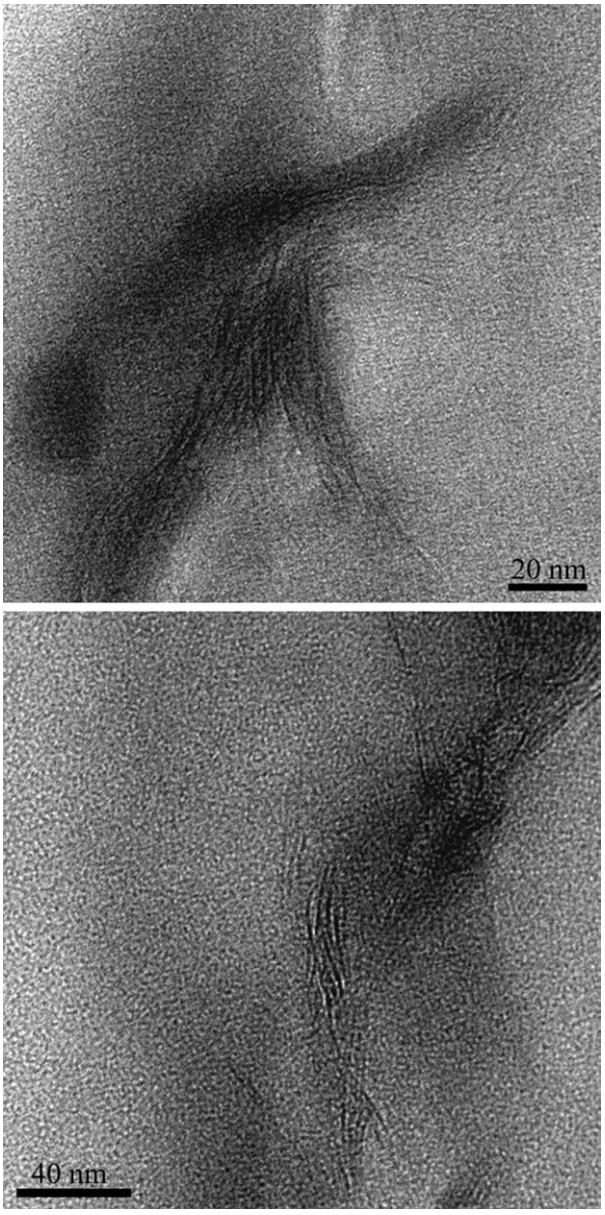

Fig. 2. TEM micrographs of the 2.8 vol% 2C18·M880-HDPE nanocomposite. The dark lines are cross-sections of the aluminosilicate layers.

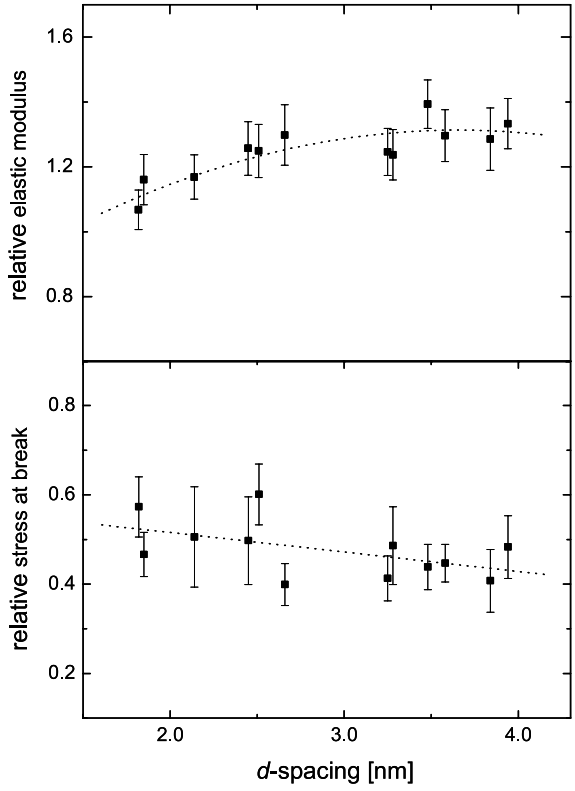

Fig. 3. The relative elastic modulus and stress at break of 2.8 vol% HDPE-OM nanocomposites plotted as a function of their *d*-spacing. The dotted lines are simply guides for the eye.

exfoliated layers are kinetically trapped in the viscous polymer melt, so that they do not collapse during compression molding. For practical purposes, this seems to be sufficient. A principal drop in the stress at break due to the presence of the filler, followed by further small decrease with increasing *d*-spacing (increasing exfoliation) was observed (Fig. 3). This is probably due to the fact that the filler is not fully delaminated. With increasing exfoliation, a monotonous increase in the yield stress and decrease in the yield strain were also observed (Fig. 4), indicating that the composites are becoming less ductile. The modest increase in yield stress suggests weak attraction forces between the OM and PE, while the decrease in yield strain is probably due to local strain amplification in the polymer confined between the particles.

Solid particles sometimes nucleate the polymer crystallization, increasing its crystallinity, decreasing crystallite thicknesses, and influencing the orientation of the lamellae in the crystallites [44,45]. This can influence the mechanical properties of the composites. However, particle anisotropy and orientation were found to have a more pronounced effect on the composite properties than heterogeneous nucleation [44]. Calorimetric measurements on the prepared HDPE-OM nanocomposites showed small differences in the polymer melt enthalpy (less than 4%) without a specific trend [46]. Therefore, the observed changes in the tensile properties cannot be due to a change in crystallinity and is more likely to be due to the presence of the inorganic inclusions, especially the highly anisotropic exfoliated silicate layers. This is in line with the finding that OMs do not significantly nucleate the crystallization of HDPE under the conditions used here [47]. The gas permeability of these nanocomposites also decreased with increasing *d*-spacing, in line with the assumption that the reinforcement is due to the presence of the inorganic inclusions and that larger *d*-spacing leads to more exfoliation [46].

The tensile properties of the 2C18·M900 nanocomposites with increasing inorganic volume fraction were measured and are summarized in Table 4. The relative

Table 3
Tensile properties of HDPE and its OM-nanocomposites (0.028 inorganic volume fraction)

Filer	Elastic modulus[a] [MPa]	Yield stress[b] [MPa]	Yield strain[c] [%]	stress at break[d] [MPa]
Neat HDPE	1020	26	9.6	36
C18·M680	1090	25	8.4	20
2C18·M680	1280	25	7.5	18
3C18·M680	1270	25	6.3	15
2C18·M880	1270	26	7.6	21
3C18·M880	1420	28	6.2	16
C18·M900	1180	25	8.8	17
2C18·M900	1320	26	6.7	14
3C18·M900	1320	28	6.3	16
4C18·M900	1360	28	5.9	17
C18·M1000	1190	24	8.7	18
2C18·M1000	1260	26	7.3	17
3C18·M1000	1310	27	6.6	15

[a] Relative probable error 5%.
[b] Relative probable error 2%.
[c] Relative probable error 5%.
[d] Relative probable error 15%.

values (composite/matrix) are plotted as a function of the filler loading in Figs. 5 and 6. Since the inorganic part of the OM is that which contributes to the reinforcement, its volume fraction was correlated with the tensile properties of the composites. With augmenting filler loading, the composites become stiffer and a 35% increase in Young's modulus is achieved at 2.8 vol% inorganic content. The relative elastic modulus is plotted as a function of the composite inorganic volume fraction and compared to the theoretical predictions in Fig. 5. As can be seen, the modulus increases monotonously with filler loading but at a higher rate than that predicted by Eq. (1), which assumes that the inclusions are spherical, underlining the anisometry of the particles. Fitting the measured data to Eq. (2) with

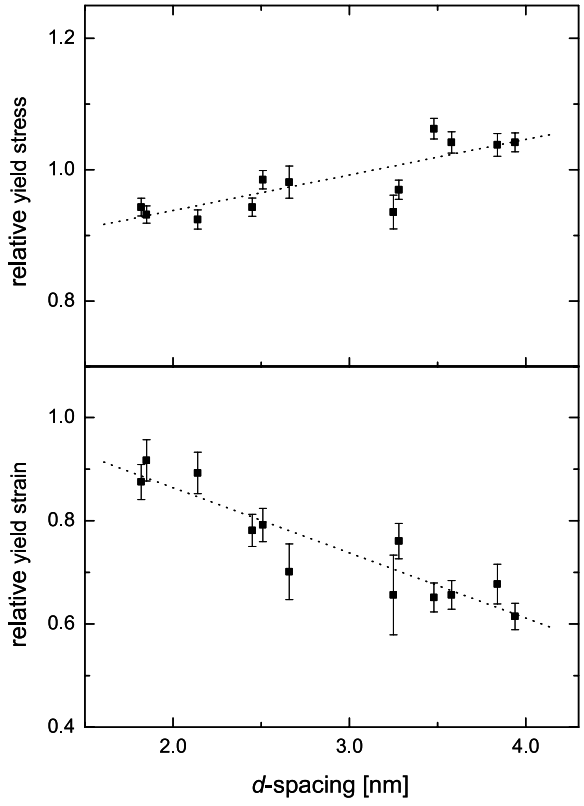

Fig. 4. The relative yield stress and strain of 2.8 vol% HDPE-OM nanocomposites plotted as a function of their *d*-spacing. The dotted lines are simply guides for the eye.

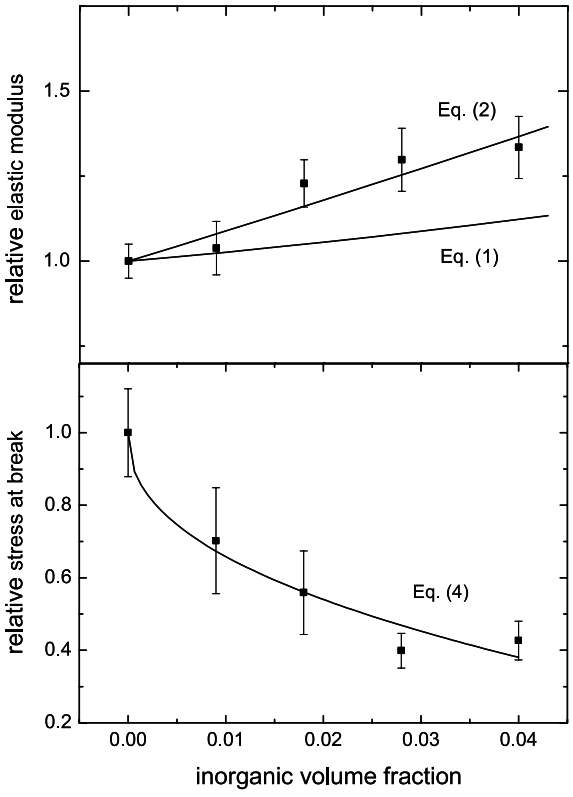

Fig. 5. The relative elastic modulus and stress at break of 2C18·M900 nanocomposites plotted as a function of their inorganic volume fraction. The solid lines represent the calculated values from the indicated equation.

Table 4
Tensile properties of HDPE and its 2C18·M900 nanocomposites as a function of filler loading

Inorganic volume fraction	Elastic modulus[a] [MPa]	Yield stress[b] [MPa]	Yield strain[c] [%]	Stress at break[d] [MPa]
0.000	1020	27	9.6	36
0.009	1060	26	9.3	25
0.018	1250	26	8.2	20
0.028	1380	26	6.6	14
0.040	1360	25	6.3	15

[a] Relative probable error 5%.
[b] Relative probable error 2%.
[c] Relative probable error 5%.
[d] Relative probable error 15%.

$B=1$, gives a value of 7.8 for parameter A, which shows that in this case it cannot be twice the aspect ratio of the inclusions as postulated by Halpin [16]. From the gas permeation measurements of these composites, a macroscopic average for the aspect ratio (diameter/thickness) was estimated to be between 50 and 150 (depending on the particle orientation) [46]. It is to be noted that the montmorillonite platelets in these composites are only partially aligned. In fact, the parameter A in Eq. (2) is a shape factor, which is not only related to the aspect ratio of the inclusions but also to their orientation with respect to the stress field and Poisson's ratio of the matrix [16,48]. Furthermore, the model assumes perfect adhesion between the inclusions and the matrix, which is not true for surface-treated fillers because only weak van der Waals attraction forces exist between the organic monolayer covering the filler surface and the polymer. It seems that it is not possible to estimate a macroscopic average of the aspect ratio for the inclusions from elastic modulus measurements, as can be done from the permeability measurements. The tensile strength of the composites decreased asymptotically with augmenting filler loading (Table 4, Fig. 5) possibly due to disabled strain hardening of the polymer in presence of the inclusions and to the presence of tactoids. Fitting the relative stress at break data to Eq. (4) (Fig. 5), gave $b=2.47$ and $a=0.43$, which deviate from the values usually obtained for spherical particles ($b=1.21$, $a=0.66$). However, the calculated value for the parameter a cannot be directly brought in connection with the aspect ratio of the inclusions. The yield stress of the composites also decayed non-linearly with increasing inorganic volume fraction and fitting the relative values to Eq. (4) (Fig. 6) resulted in $b=12.6$ and $a=1.7$. This is in contrast to the results reported by Hotta and Paul [30], where better exfoliation was achieved in presence of maleic anhydride-grafted PE, showing that the decrease in yield stress is probably due to the presence of tactoids. The yield strain also decreased monotonously with increasing filler loading and the stress–strain curve indicated increasing brittleness.

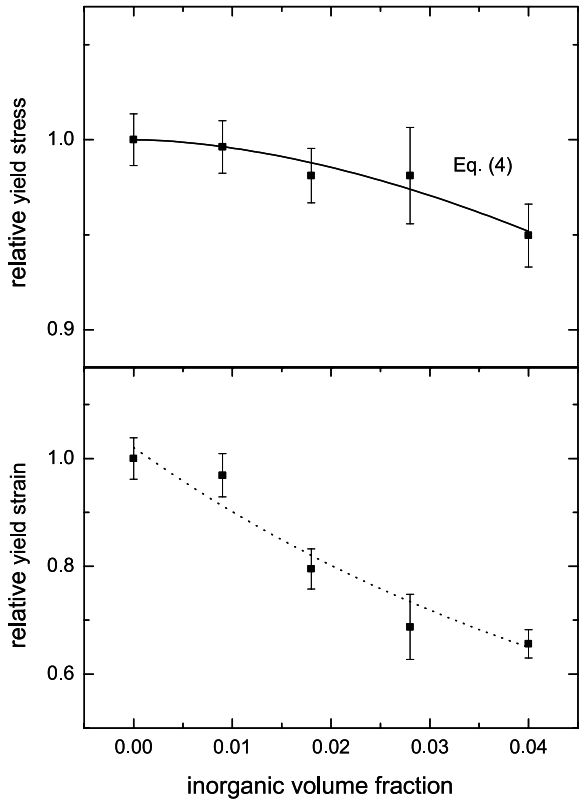

Fig. 6. The relative yield stress and strain of 2C18·M900 nanocomposites plotted as a function of their inorganic volume fraction. The solid line represents the calculated yield stress values from Eq. (4), while the dotted line is simply a guide for the eye.

4. Conclusions

A high cation cross-sectional area to available area ratio in the organic monolayer of the OM is necessary to organophilize the montmorillonite surface and to attain large d-spacing favorable for exfoliation. An identical chemical structure of the organic monolayer and the polymer as well as large d-spacing does not lead to complete exfoliation, if the free energy of mixing is still high. Partial exfoliation leads to an appreciable increase in the elastic modulus of the nanocomposites at low filler loading. The modulus-composition dependence cannot be used to estimate a macroscopic average for the inclusions' aspect ratio from the Halpin-Tsai equation because the composite modulus depends also on the particle orientation

and Poisson's ratio of the matrix. High shear rates during compounding OMs with large *d*-spacing, that lead to improved exfoliation are expected to enhance the mechanical performance of nanocomposites.

Acknowledgements

We gratefully acknowledge financial support from the Swiss National Science Foundation (SNF) and from TOP NANO 21 of the ETH Board. We also would like to thank NESTEC, Lausanne and ALCAN PACKAGING, Neuhausen for supporting the project.

References

[1] Katz HS, Milewski JV, editors. Hand book of fillers for plastics. New York: Van Nostrand Reinhold Company; 1987.
[2] Jancar J, editor. Mineral fillers in thermoplastics. Advances in polymer science, vol. 139. Berlin: Springer; 1999.
[3] Malik TM, Faroqi MI, Vachet C. Polym Compos 1992;13:174.
[4] Osman MA, Atallah A, Müller M, Suter UW. Polymer 2001;42(15): 6545.
[5] Pukánszky B. Polypropylene structure, blends and composites. vol. 3. London: Chapman and Hall; 1995.
[6] Vollenberg PHT, Heikens D. Polymer 1989;30:1656.
[7] Bartczak Z, Argon AS, Cohen RE, Weinberg M. Polymer 1999;40: 2347.
[8] Pukánszky B. New Polym Mater 1992;3:205.
[9] Fu Q, Wang G, Liu C. Polymer 1995;36(12):2397.
[10] Smallwood HM. J Appl Phys 1944;15:758.
[11] Guth E. J Appl Phys 1945;16:20.
[12] Kerner EH. Proc Phys Soc 1956;B69:808.
[13] Hashin Z, Shtrikman S. J Mech Phys Solids 1963;11:127.
[14] Halpin JC. J Composite Mater 1969;3:732.
[15] Halpin JC, Kardos JL. Polym Eng Sci 1976;16:344.
[16] Halpin JC. Primer on composite materials analysis. Lancaster: Technomic; 1992.
[17] Nicolais L, Nicodemo L. Polym Eng Sci 1973;13:469.
[18] Giannelis EP. Adv Mater 1996;8:29.
[19] LeBaron PC, Wang Z, Pinnavaia TJ. Appl Clay Sci 1999;15:11.
[20] Alexandre M, Dubois Ph. Mater Sci Eng R 2000;28:1.
[21] Osman MA, Mittal V, Morbidelli M, Suter UW. Macromolecules 2003;36:9851.
[22] Gilman JW, Jackson CL, Morgan AB, Harris R, Manias E, Giannelis EP, Wuthenow M, Hilton D, Phillips SH. Chem Mater 2000;12:1866.
[23] Jasmund K, Lagaly G, editors. Tonminerale und Tone. Darmstadt: Steinkopff; 1993.
[24] Osman MA, Plötze M, Suter UW. J Mater Chem 2003;13:2359.
[25] Bergman JS, Chen H, Giannelis EP, Thomas MG, Coates GW. Chem Commun 1999;21:2179.
[26] Heinemann J, Reichert P, Thomann R, Mülhaupt R. Macromol Rapid Commun 1999;20:423.
[27] Alexandre M, Dubois P, Sunb T, Garcesb JM, Jérôme R. Polymer 2002;43:2123.
[28] Kato M, Okamoto H, Hasegawa N, Tsukigase A, Usuki A. Polym Eng Sci 2003;43:1312.
[29] Liang G, Xu J, Bao S, Xu W. J Appl Polym Sci 2004;91:3974.
[30] Hotta S, Paul DR. Polymer 2004;45:7639.
[31] Fornes TD, Yoon PJ, Keskula H, Paul DR. Polymer 2001;42:9929.
[32] Fornes TD, Paul DR. Polymer 2003;44:4993.
[33] Vaia RA, Giannelis P. Macromolecules 1997;30:7990.
[34] Balazs AC, Singh C, Zhulina E, Lyatskaya Y. Acc Chem Res 1999; 32:651.
[35] Ginzburg VV, Singh C, Balazs AC. Macromolecules 2000;33:1089.
[36] Borukhov I, Leibler L. Macromolecules 2002;35:5171.
[37] Maas JH, Fleer FA, Leermakers FAM, Cohen Stuart MA. Langmuir 2002;18:8871.
[38] Osman MA, Ernst M, Meier B, Suter UW. J Phys Chem B 2002;106: 653.
[39] Osman MA, Ploetze M, Skrabal P. J Phys Chem B 2004;108:2580.
[40] Osman MA, Ploetze M, Suter UW. J Mater Chem 2003;13:2359.
[41] Morgan AB, Harris JD. Polymer 2003;44:2313.
[42] Osman MA, Atallah A, Suter UW. Polymer 2004;45:1177.
[43] Osman MA, Mittal V, Morbidelli M, Suter UW. Macromolecules 2004;37:7250.
[44] Pukánszky B, Belina K, Rockenbauer A, Maurer FHJ. Composites 1994;25:205.
[45] Bartczak Z, Argon AS, Cohen RE, Kowalewski T. Polymer 1999;40: 2367.
[46] Osman MA, Rupp JEP, Suter UW. J Mater Chem (submitted for publication).
[47] Osman MA, Atallah A. Macromol. Rapid Commun 2004;25:1540.
[48] Kuelpmann A, Osman MA, Kocher L, Suter UW. Polymer 2004;46: 523.